

FAST NEUTRON TIME ENCODED IMAGING FOR SPECIAL NUCLEAR MATERIAL DETECTION

Aaron Nowack, Jim Brennan, Erik Brubaker, Mark Gerling, Peter Marleau, Kyle McMillan,
Patricia Schuster, John Steele
Sandia National Laboratories
P.O. Box 969, MS-9506, Livermore, CA 94551-0969

ABSTRACT

Rising concerns in monitoring the presence and movement of special nuclear material (SNM) highlight the need for improved reliable neutron detection methods for large standoff distances. To be incorporated as a deployable system, standoff detection methods must be efficient and cost-effective, feature good signal to background discrimination and accurately identify the presence and location of material. By decoupling the desired features of a standoff detector from each other, they can be optimized independently. Time-encoded imaging (TEI) separates source position and signal to background discrimination from the detector through the use of time-modulated collimators. This allows high angular resolution while greatly increasing efficiency and energy resolution by relying on single scatters of fast neutron and gammas in a large scintillator volume. This paper presents results using two prototype detectors based on time-encoded imaging for fission neutron detection in realistic standoff scenarios. A new extension to high-resolution two-dimensional imaging is also presented. These results showcase the ease of deployment for TEI detector systems due to their lower cost, reduced complexity, and scalability.

INTRODUCTION

The detection of nuclear materials at large stand-off distances has applications in nuclear security and counter-terrorism programs. At these distances a detector must rely on either fast neutrons or gamma rays as the signatures of nuclear material due to their high penetrating power. Compared with gammas, fast neutrons have a relatively low and understood background. This provides an ideal regime for detection of special nuclear material in large search area scenarios.

Thus far two approaches compose most fast neutron imagers. Traditional coded apertures are based on a front pixelated mask plane of hydrogenous material and a detector array as the rear plane (1). The pattern of the mask plane is based on Uniformly Redundant Arrays (URAs) which have a mathematical property to uniquely reconstruct the spatial distribution of a source under ideal imaging conditions. In addition, optimized random masks are also used. However in practice the construction and calibration of large detector arrays impact cost and performance of these detectors. A second approach replaces the front mask plane with another large detector plane and looks for coincidence scatters in the front and rear, known as a scatter camera (2). The direction of an incoming neutron is constrained and can map out a source distribution. This setup has been shown to be successful in near and medium distance regimes, however the requirement of double scatters greatly reduces efficiency and increases necessary dwell time for long-range detection.

Time-encoded imaging (TEI) is a new method for SNM detection with fast neutrons that overcomes the limiting factors for both of these previous approaches. The concept relies on measuring the presence of a nuclear source as a time varying neutron rate as it is modulated by shielding material moving around each detector. TEI designs feature simple construction reducing cost and complexity

while maintaining a high efficiency by requiring only single scatters. Additionally by converting spatial variations into temporal rates the system is more robust against non-uniformities in the detected background due to detector geometry. For these reasons TEI detectors offer simple, low-cost, and highly efficient solutions for detecting SNM. There has been previous work on the related technique of Rotating Modulated Collimators (RMC) for security applications (3)(4). While incorporating some of the advantages of a TEI design, the RMC is not suitable for fast neutrons because the required thick masks significantly reduce the efficiency of the imager.

PROTOTYPE DESIGN

Two prototype designs were built for performance comparisons and have been described previously (5). The prototypes are shown in Figure 1. Both designs use rotating elements to induce modulation in the neutron signal as a function of rotation angle. These prototypes have proved to be pivotal in the development of more sophisticated long-range detector designs.



Figure 1: Left: The LIGHTHOUSE detector built from a rotating mask of High Density Polyethylene (HDPE) with a single 5” liquid scintillator cell and photo-multiplier tube (PMT) in the center. Right: The PRISM detector consisting of three large cells each housing liquid scintillator and a 9” PMT rotating on a central axis.

The first prototype, referred to as LIGHTHOUSE, is composed of a central detector surrounded by an order 31 mask of collimators and gaps in an URA pattern. The detector is approximately one half-liter volume of EJ301 liquid scintillator coupled to a 5” Hamamatsu R1250 PMT. The rotating collimator consists of 3.5”x3.5”x27” HDPE bars hanging vertically from a steel ring frame. The frame is driven by an electric motor whose position is recorded with a digital encoder and recorded with a data acquisition system (DAQ) that records full digitized waveforms of the PMT pulses.

The second prototype, the Portable Rotating Imager using Self Modulation (PRISM) is composed of several detectors cells, each acting as an active collimator for adjacent cells as they rotate around a common central axis. Each of the PRISM cells are housed in a 12” diameter aluminum can filled with ~27 liters of liquid scintillator (EJ309). A 9” Photonis XP1802 PMT is in contact with the scintillator and is secured and sealed with several O-rings 15” from the bottom of the can.

Both imager prototypes are triggered with an analog MPD4 module and readout using a Struck SIS3350 500 MS/s waveform digitizer.

CELL PERFORMANCE

Large volumes of scintillator are necessary for detecting neutron sources at large standoff distances because of the very low neutron flux reaching the detector. For example, at 100 m the fast neutron flux of an IAEA significant quantity of weapons-grade plutonium (WGpu) is ~ 1.3 neutrons/s/m², assuming an attenuation length in air of ~ 100 m. The standoff detection problem therefore requires several large and efficient detectors. Detector performance must be balanced against total volume. Large detectors are exposed to more neutrons, but often have worse light collection and pulse shape discrimination, with a correspondingly higher effective threshold. A comparison between LIGHTHOUSE and PRISM can help quantify the tradeoff between cell volume and performance.

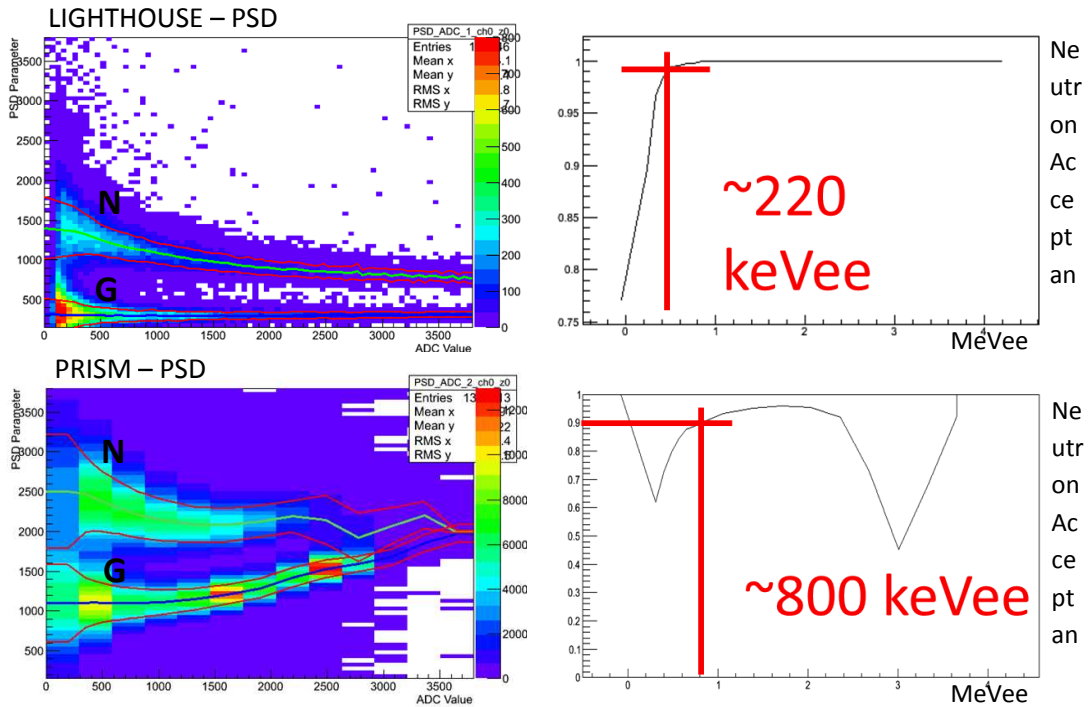


Figure 2: Neutron/gamma discrimination in the LIGHTHOUSE (top) and PRISM (bottom) liquid scintillator cells. Left: PSD is plotted against pulse height: the amount of separation in the neutron and gamma bands measures the efficiency of the cell to discriminate between the particles. Right: Neutron efficiency as a function of recoil proton energy for our PSD cut.

A threshold is placed requiring that events are neutrons with 99% confidence based on the ratio of the tail integral to total pulse integral. Poorer pulse-shape discrimination (PSD) performance in the PRISM cell, as shown in Figure 2, is due to variation of response across the PMT photocathode, worse transit time resolution, and worse light collection due to the large cell size. These effects can significantly reduce the neutron/gamma discrimination efficiency. This leads to an effective ~ 800 keVee (keV electron equivalent energy) threshold on the observed recoil proton energy, thus removing a large fraction of the fission spectrum. Solutions are being considered to lower the threshold in the next design as the ~ 50 times increase in scintillator volume over the LIGHTHOUSE cell remains an advantage.

SIMULATIONS

Simulations using Monte Carlo N-Particle X (MCNPX)/Polimi were analyzed to model the detector response. Several parameters are fed into a template MCNP card to vary parameters including detector geometry, source position and rotational angle of the detector. The observed rate of neutron interactions in the detectors over runs at different angles determines the rotational response of the detectors and can be used in source detection and imaging. An example is shown in Figure 3.

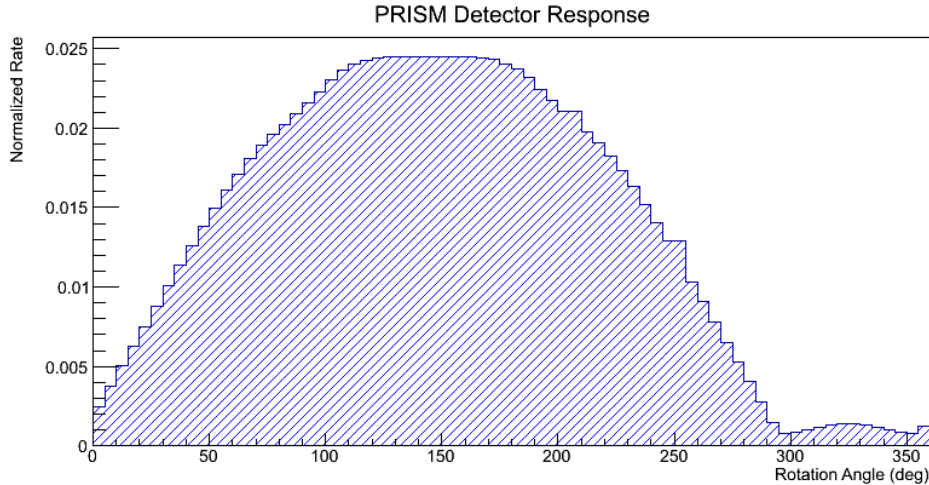


Figure 3: The normalized detector response for one of the PRISM cells from the MCNP simulations displaying the angle-dependent neutron rate modulation.

The simulations require the measured thresholds in detector cells based on PSD calibrations. Double scatters between detector pairs were also tallied but they account for only 1/4000 of the total data and are not considered in the following analysis.

RESULTS

Data is taken in list mode and is analyzed. The data and simulated detector response are combined to yield an estimated source distribution through a Maximum Likelihood Estimation Maximization (MLEM) method. This is a mature imaging method originally developed for use in medical imaging that calculates the most likely distribution and strength of a source.

Early data was taken with a ^{252}Cf source of strength comparable to an IAEA significant quantity of WGPu at 60 m. However, due to large amount of deadtime caused by the DAQ readout to disk more quantified measurements could not accurately be made. In addition it was discovered that the large PMTs in the PRISM cell are sensitive to geomagnetic fields which change the internal gain of the PMT as a function of angle. This is seen as a false modulation in background events. Despite these issues we were able to see a modulation pattern in the neutron rate matching the source position (Figure 4).

Subsequent tests were performed at a shorter stand-off distance of 5m using a $6\mu\text{Ci}$ source of ^{252}Cf in order to fully characterize the detector performance. The electronics were altered to significantly reduce the deadtime and the PRISM cell was wrapped in MuMetal to shield external magnetic fields from affecting PMT gain. Modulation patterns and reconstructed source distributions are shown in Figure 5 for this experimental configuration.

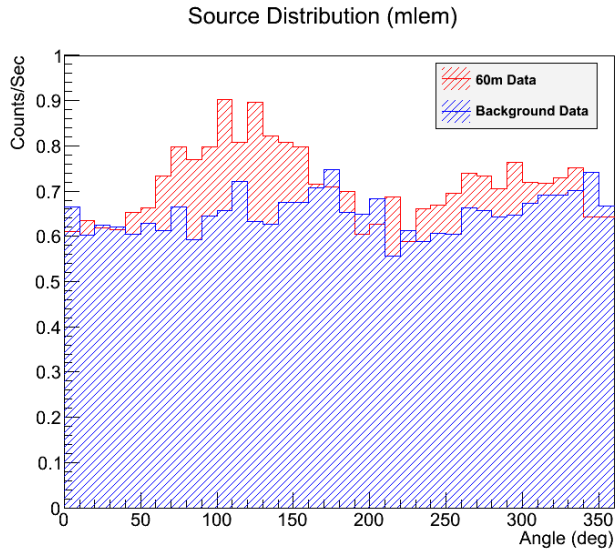


Figure 4: Observed modulation in the neutron rate as measured by PRISM for a ^{252}Cf source placed at 60 m. The neutron flux of the source is comparable to an IAEA significant quantity of WGPu.

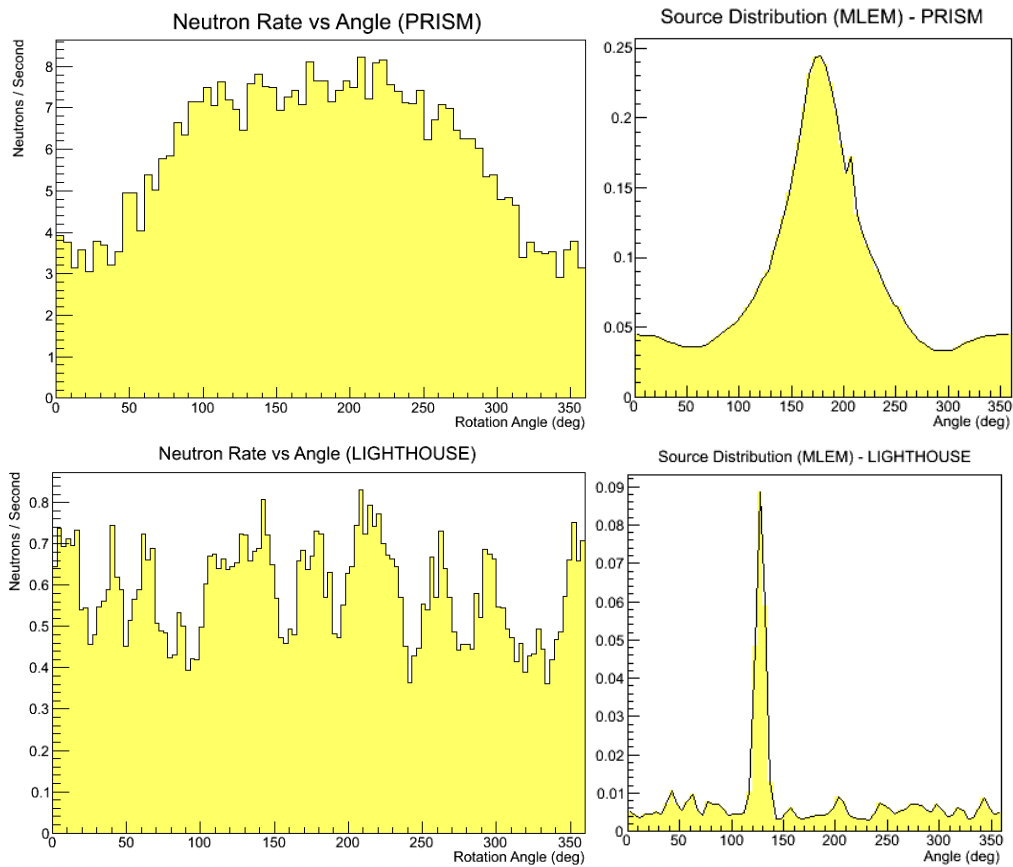


Figure 5: The observed neutron rates and corresponding MLEM source reconstruction as observed by PRISM (top) and LIGHHOUSE (bottom) for a $6\mu\text{Ci}$ source of ^{252}Cf at 5 m.

Instead of using the MLEM reconstruction to determine the presence or absence of a source over background, we ask whether a source is present within the data through a hypothesis test. Signal and background runs are decomposed into many sets of data for different dwell times. These are fed into a hypothesis test routine which measures the maximum Log-Likelihood Ratio (LLR) between the signal and background runs over possible source positions and strengths. By comparing the LLR distributions for background and signal runs the probability of correctly or falsely identifying a source can be measured. These are visualized using Receiver-Operator Characteristic (ROC) curves plotting these statistics against each other as detection threshold on the LLR is changed.

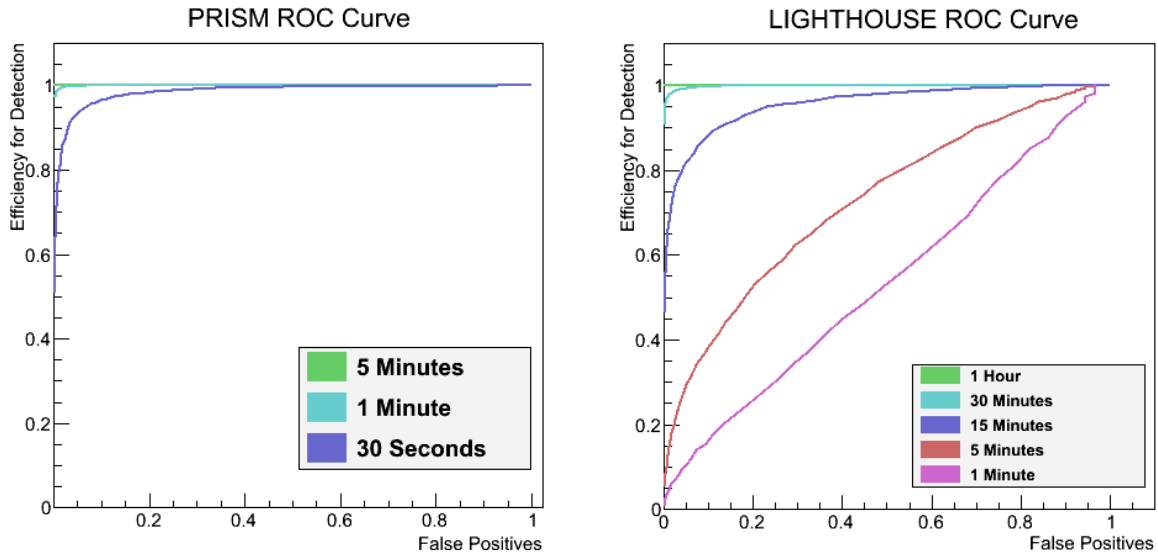


Figure 6: Comparisons between the PRISM cell and LIGHTHOUSE based on ROC curves. Probability of source detection and false identification are plotted against one another for determining whether a source is present varies. A step function would represent a perfectly ideal detector.

The ROC curve comparisons indicate that a 30-second PRISM run is near equivalent to 1200-seconds in LIGHTHOUSE, a 40x increase. The increased neutron rate between the detectors provides a factor of 10, the remaining factor of 4 is a combination of the modulation pattern providing a better signal discrimination and LIGHTHOUSE being influenced by neutrons scattering within the mask before detection.

FUTURE DESIGN

Due to the observed performance of PRISM over LIGHTHOUSE despite the much higher threshold due to poorer PSD, a new detector is being constructed based on the PRISM design. Better performance can be achieved by increasing cell size, improving PSD, and by optimizing the modulation pattern. We have examined the PSD performance of a similar 10” PMT for use in a larger cell, but calibrations indicate that the PSD performance is very poor. Other alternatives are also being tested.

Optimization of the PRISM geometry is done by examining possible setups in MCNPX and using the output detector response with the ROC curve analysis for measuring performance between geometries for equal dwell times with a source at 60 m

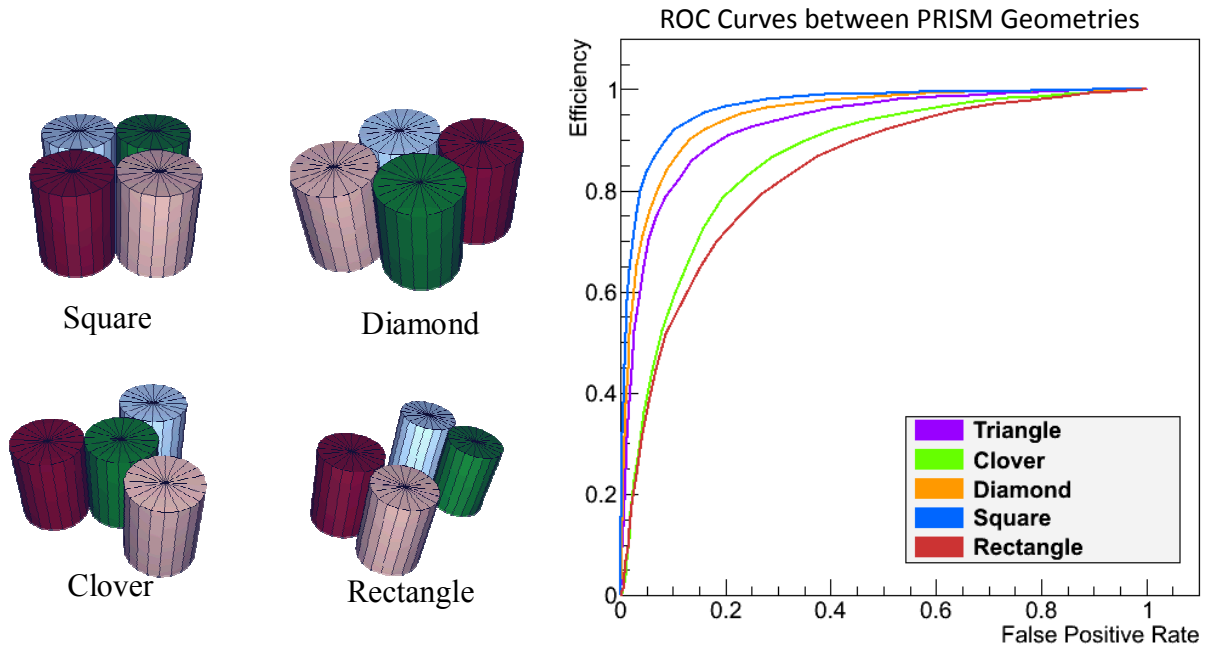


Figure 7: Comparisons between the different considered geometries (left) are compared by measuring their relative performance represented as ROC curves (right). Triangle refers to the original three cell close-packed setup.

Initially we expected performance to scale with effective detector area. However our analysis (Figure 7) indicate the opposite is true and that compact and close-packed detectors, with the smallest effective areas, perform better than detectors with more space in between such as the rectangular setup or those with significantly different modulation patterns between cells represented by the clover setup.

We are currently constructing a configurable detector with cells that can be re-position into different geometries. Our analysis indicates that a square configuration is optimal but this will be verified experimentally.

EXTENDING TO 2-D TEI IMAGERS

Based on previous work involving coded apertures for high-resolution 2-D neutron imaging, we examined whether it is possible to adapt that work into a TEI system using a single detector. By using a single detector for source detection many complexities involved with traditional coded apertures are removed. However, angular resolution is influenced by the size of the detector and consequently a TEI system with high resolution will have low effective area.

Our simulated coded-mask (Figure 8) consists of a grid of HDPE pixels arranged in either a URA or optimized random pattern. The mask is spun around the center, forming a modulated pattern which depends on the detector and source positions.

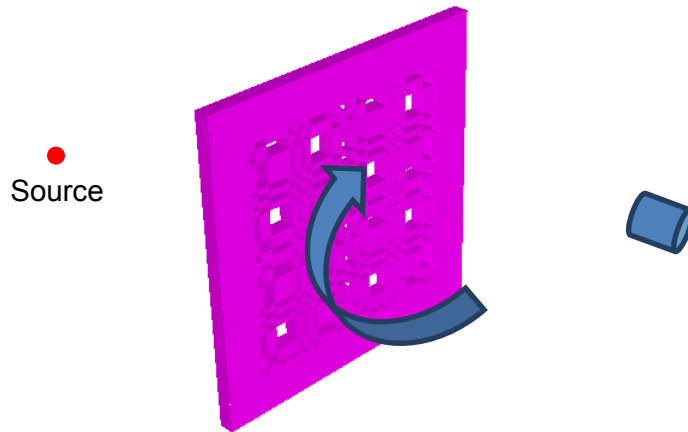


Figure 8: A simulated spinning aperture for 2D TEI imaging. A single detector (right) observes a modulation pattern dependent on the position of the source (left).

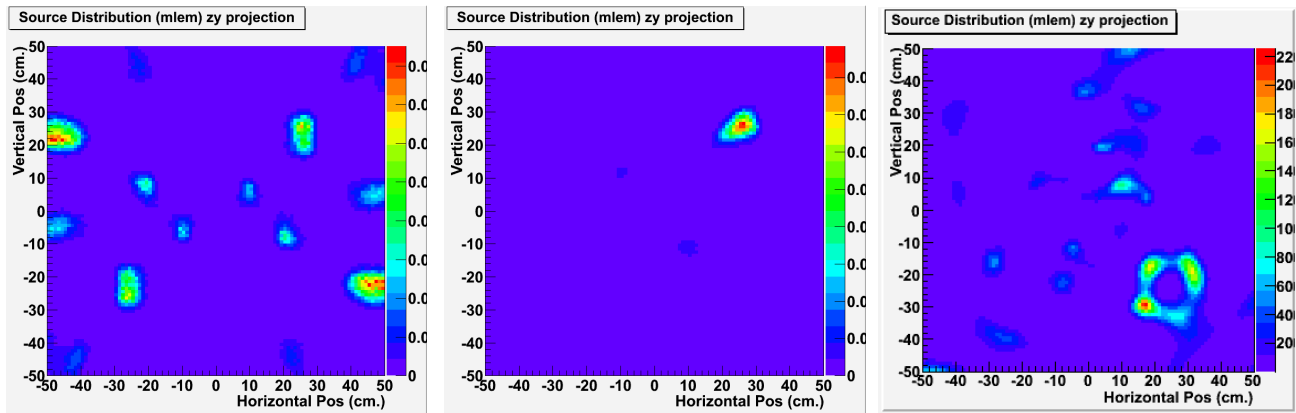


Figure 9: Results of the MLEM reconstruction for several different setups at 1000 second exposures. (Left) Image of a source at (25cm, 25cm) using a URA mask pattern. (Middle) Same setup as left image but with an optimized random pixelated grid. (Right) An optimized random grid image of a thin ring source at (25cm, -25cm).

Initial results are promising (Figure 9) and show the possibility of high resolution 2D imaging with a single detector. For the URA pattern many artifacts arise, however based on previous experience with URAs in coded masks this is not a surprising result. A previously derived random mask optimized for traditional coded apertures was also used and for point and extended sources displayed promising reconstructed images. There are distortions for sources near the center of the mask due to low modulation in the mask pattern. Configurations involving more than one detector will be investigated. Further research is underway for a variety of 2-D TEI imaging configurations.

CONCLUSIONS

We have introduced the TEI design and shown its advantages in detecting SNM at large distances. TEI offers a cost-effective means of detecting and imaging radioactive sources and is easily deployable. A new one dimensional detector based on the results of PRISM that will optimize the geometry and incorporate better PSD to lower thresholds is planned. Future work on extensions of TEI into two dimensions are promising and further research is underway.

REFERENCES

1. M.A. Blackston, B.L. Brown, E. Brubaker, P.A. Hausladen, P. Marleau, J. Newby, "Fast Neutron Coded Aperture Imaging for Warhead Counting," INMM 2011, Desert Springs, CA
2. J. Brennan, R. Cooper, M. Gerling, P. Marleau, N. Mascarenhas, and S. Mrowka, "Results with a 32-element dual mode imager," IEEE NSS Conference Proceedings, 2010, pp. 1634-1639.
3. B.R. Kowash, D.K. Wehe, and J.A. Fessler, "A rotating modulation imager for locating mid-range point sources," Nuclear Instruments and Methods in Physics Research Section A, 602, 2009.
4. B. O. Nathan, B. R. Kowash, and D. K. Wehe, "Thermal neutron imaging with a Rotationally Modulated Collimator (RMC)," IEEE NSS Conference Proceedings, 2009, pp. 1129-1133.
5. P. Marleau, "Time Encoded Fast Neutron/Gamma Imager for Large Standoff SNM Detection," IEEE NSS Conference Proceedings, 2011, pp. 591-595.